

Anomalous Magnetoresistance by Breaking Ice Rule in $\text{Bi}_2\text{Ir}_2\text{O}_7/\text{Dy}_2\text{Ti}_2\text{O}_7$ Heterostructure

H. Zhang^{1†}, K. Noordhoek^{1†}, C. K. Xing^{1†}, T. H. Zhao², L. Horák³, Q. Huang¹, L. Hao¹, J. Yang¹, S. Pandey¹, E. Dagotto^{1,4}, Z. G. Jiang², E. S. Choi⁵, H. D. Zhou^{1*} and J. Liu^{1*}

¹Department of Physics and Astronomy, University of Tennessee, Knoxville, TN, USA, 37996

²School of Physics, Georgia Institute of Technology, Atlanta, GA, USA, 30332

³Charles University, Prague, Czechia, 11636

⁴Materials Science and Technology Division, Oak Ridge National Laboratory, Oak Ridge, TN, USA, 37831

⁵National High Magnetic Field Laboratory, Tallahassee, FL, USA, 32310

Abstract

While extensive studies on geometrically frustrated quantum magnets with exotic spin states show promises for quantum computing and quantum information technologies, most of them are good insulators which are difficult to be integrated with modern electrical circuit that relies on moving charge carriers. The grand challenge is to find a way to introduce interactions between the localized spins and charge carriers and convert the spin excitations into electronic responses. Here, we show that by designing a $\text{Bi}_2\text{Ir}_2\text{O}_7/\text{Dy}_2\text{Ti}_2\text{O}_7$ heterostructure, the breaking of the ice rule in the spin ice $\text{Dy}_2\text{Ti}_2\text{O}_7$ can lead to a charge response in the $\text{Bi}_2\text{Ir}_2\text{O}_7$ conducting layer that can be detected as anisotropic magnetoresistance. These results demonstrate a novel and feasible approach for probing interactions between charge carriers and exotic spin states in insulating magnets, which lays out a blueprint for metallization of quantum magnets.

†equal contribution; *corresponding author

Novel emergent states of quantum magnets often arise from geometric frustration, where local spins residing on the corners of a triangle or tetrahedron cannot agree on a unique alignment that simultaneously minimizes their energies¹. Such a spin lattice has a large degree of degeneracy as enormous configurations share the same or similar energy, leading to exotic ground states, entangled fluctuations, and collective excitations^{2, 3, 4, 5}. The so-called dipolar spin ice is one of the most important representatives of such frustrated magnets. It was first discovered on pyrochlore lattice of Ising spins constrained along the local [111] direction, such as $\text{Ho}_2\text{Ti}_2\text{O}_7$ and $\text{Dy}_2\text{Ti}_2\text{O}_7$ (DTO)^{6, 7, 8, 9, 10}. When the spin-spin correlation is dominated by the dipolar interaction, the ferromagnetic instability is geometrically frustrated by the local Ising anisotropy¹¹. As a result, the ground state of each tetrahedron settles in one of the six-fold degenerate 2-in-2-out configurations, forming a spin ice network throughout the lattice following the ice rule in analog with the proton displacement in the water ice shown in figure 1(a). Non-zero residue entropy has indeed been observed with a value close to that in the water ice¹². Breaking the ice rule could lead to rich spin dynamics. For instance, applying a magnetic field along a [111] direction in DTO creates emergent magnetic monopoles¹³, turns the three-dimensional spin ice into a Kagome spin ice¹⁴, and eventually stabilizes the 3-in-1-out or 1-in-3-out configuration, giving rise to a jump from $\sim 3.3 \mu_B/\text{Dy}$ to $\sim 5 \mu_B/\text{Dy}$ between two magnetization plateaus^{15, 16, 17}.

The spin-ice behaviors have however been only observed in highly insulating compounds where the spins are carried by highly localized electrons in the absence of other itinerant carriers, such as the *f*-electrons of Ho^{3+} or Dy^{3+} ions in combination with the empty *d*-shell of the Ti^{4+} valence state in the pyrochlore titanates^{6, 7, 8, 9, 10}. While it is an interesting open question to see whether and how the spin ice state would interact with itinerant carriers and introduce any novel electronic behaviors, simply replacing the B-site with another element with a metallic configuration often ends up destroying the spin ice state^{18, 19}. For instance, the correlated *d*-electrons in pyrochlore iridates not only exhibit their own magnetic instability with an all-in-all-out ordering at much higher temperatures, but also force the same magnetic order onto the rare earth sublattice^{20, 21, 22, 23, 24, 25}. Although the rare earth moments may in turn modify the transport properties of the *d*-electrons²⁶, the physics is still dictated by the energy scale of the spontaneous magnetic order of the *d*-electrons, which is much larger than the interaction within the rare earth sublattice. This issue indeed applies to a broader class of frustrated magnets beyond spin ice.

In this work, we report observation of an anomalous magnetoresistance (MR) in epitaxial pyrochlore heterostructures of $\text{Bi}_2\text{Ir}_2\text{O}_7/\text{Dy}_2\text{Ti}_2\text{O}_7$ (BIO/DTO), where DTO hosts the spin ice state and BIO, the only nonmagnetic/time-reversal-invariant member of the pyrochlore iridate series, provides the correlated carriers. We directly grow ultrathin films of BIO on DTO single crystals, a schematic graph is shown in figure 1(b). An anomalous feature in the MR is observed, when the field is applied along the [111] direction, and corresponds to the transition between the Kagome spin ice state and the 3-in-1-out state. When we further synthesize the BIO/DTO heterostructure on Ytria Stabilized Zirconia (YSZ) substrate with DTO also grown as a thin film, the anomalous feature appears at a higher field, indicative of strain-tuning of the spin ice state. These results demonstrate that epitaxial interface is an effective approach to induce interactions between charge carriers and exotic spin states in insulating frustrated magnets.

The single crystal DTO was prepared by the floating zone method²⁷. The crystal was first oriented and cut into substrate pieces along the DTO (111) lattice plane. The substrate surface was then polished through a five-step process (see details in experimental method) to achieve atomically flat surfaces. Figure 1(c) shows a typical atomic force microscope (AFM) image of the DTO single crystal substrate after the process. A thin layer of 3 – 5 nm BIO was deposited on the DTO substrate by pulsed laser deposition²⁸. Figure 1(d) shows a typical specular x-ray diffraction scan covering the DTO [222] to [444] structural peaks. The corresponding peaks of BIO can also be seen near each DTO peak with much smaller intensities as expected. Reciprocal space mapping (RSM) shows that the BIO film of such thickness is in a fully strained state (supplementary).

While most members of the pyrochlore iridate series exhibit the all-in-all-out magnetic ordering of the Ir pseudospin-1/2 electrons with an ordering temperature decreasing with the increasing A-site ionic radius^{29, 30}, BIO is a bad metal on the paramagnetic side of the quantum critical point³¹. No magnetic ordering or spontaneous time-reversal-symmetry-breaking was found down to 50 mK³². Moreover, it has been shown that, although the BIO metallicity will degrade when grown as ultrathin films likely due to weak localization and/or disorder-enhanced electron–electron interaction in two-dimensions, the highly isotropic MR with respect to different crystallographic axes is robust against the dimensional reduction and characteristic of spin fluctuation³³. Our ultrathin BIO films on DTO indeed show a weakly increasing resistivity

as lowering temperature as well as an isotropic MR above 2 K (supplementary), consistent with previous reports^{33, 34}. However, an emergent anisotropy of the MR was observed when measuring at lower temperatures. Figure 2(a)(b) shows representative MR curves as a function of magnetic field \mathbf{H} applied along the [111] and [1-10] directions at 0.3 K with the current being kept perpendicular to the field. While the overall MR response is negative for both directions, the MR curve with $\mathbf{H}//[111]$ clearly shows an anomaly that is maximized around 1.4 T and absent with $\mathbf{H}//[1-10]$. Such anisotropic MR of the BIO layer is an indication of influence from DTO.

To gain more insight of the observed MR anomaly, we performed ac susceptibility measurement at the same temperature, which is expected to be dominated by the DTO substrate. The result in the middle panel of figure 2(b) shows a clear sharp peak when $\mathbf{H}//[111]$ at the same field where the MR anisotropy is maximized, indicating a magnetic transition. It is, on the other hand, featureless for $\mathbf{H}//[1-10]$. This observation is consistent with the well-established transition from the Kagome spin ice to the 3-in-1-out state of DTO when $\mathbf{H}//[111]$ ¹⁶. The critical field value here is slightly bigger than reported intrinsic value ~ 1 T^{15, 16} due to the demagnetization effect of our substrate which is cut as a thin rectangular plate.

Nevertheless, the MR anomaly in the BIO layer with $\mathbf{H}//[111]$ is clearly associated with the breaking of the ice rule in the DTO, indicating that the charge carriers of BIO are sensitive to the spin state in DTO through the interfacial coupling with the local moments. We verified these observations by measuring a reference sample where the BIO film was deposited on a (111)-oriented $\text{Y}_2\text{Ti}_2\text{O}_7$ single crystal substrate. Indeed, as shown in the bottom panel of figure 2(b), the isotropic MR between $\mathbf{H}//[111]$ and $\mathbf{H}//[1-10]$ fully recovers with the absence of the 1.4 T anomaly in this reference system where Dy is replaced with the nonmagnetic Y ion and the interface coupling is removed. We further studied the thermal evolution of this anisotropic MR feature between 0.3 K and 0.9 K. The result displayed in figure 2(c) shows that the anomaly decreases with increasing temperature and starts to vanish at 0.9 K. This is consistent with the reported melting of the spin ice state in DTO due to thermal fluctuation¹².

Having confirmed these observations, we exploited the sensitivity of the BIO layer to the breaking of the ice rule to investigate potential differences in DTO thin films. This is motivated by the fact that, while a number of recent studies on thin films of spin ice materials have

suggested that epitaxial strain could be an effective knob to modulate the exchange interactions, the degree of frustration, and the emergent magnetic state^{35, 36, 37}, the magnetic behaviors have been difficult to probe in thin films samples due to the limited volume. We synthesized bilayer heterostructures of BIO and DTO, where a DTO layer of 20 – 25 nm is also grown along the [111] direction on (111)-oriented Yttria Stabilized Zirconia (YSZ) single crystal substrates. A schematic diagram is shown in figure 3(a). This thickness is chosen to avoid relaxation. The x-ray characterization indeed shows a fully strained state for both the DTO and BIO layers (supplementary information), where the DTO has a 0.8% lattice mismatch with YSZ and is compressed epitaxially by ~ 3.2%. Similar to the samples grown on DTO crystals, transport measurement of the BIO layer also shows a weakly semiconducting behavior and an isotropic MR at high temperatures (supplementary information). When measuring at lower temperature with a magnetic field $H // [111]$ and $H // [1-10]$, anisotropy emerges as well in the MR. Figure 3(b) shows the MR measured at 0.3 K. When the external magnetic field is along the local [111] direction, the MR curve of the BIO/DTO/YSZ sample is seen to exhibit a hump maximized around 2.8 T, which is absent when the field is applied along the [1-10] direction. The emergence of such an anisotropic MR anomaly is similar to that in the BIO/DTO but at a much larger field. To ensure its magnetic nature, we synthesized another heterostructure where the spin ice DTO is again replaced by the non-magnetic $Y_2Ti_2O_7$ (YTO) as a reference. The result, displayed in the bottom panel of figure 3(b), shows that the MR in this case is identical and featureless when the magnetic field is applied along the [111] and [1-10] direction. This comparison confirms that the anisotropic MR feature in the BIO/DTO/YSZ is due to the breaking of the ice rule and the transition to the 3-in-1-out state with the increasing field.

To further investigate the nature of this anisotropic MR feature, we conducted a series of measurement between 0.03 K and 0.95 K. The result in figure 3(c) shows that the amplitude of the hump keeps decreasing with increasing temperature without any obvious shift in field. It disappears when temperature increases to above ~0.6 K, where the two MR curves become overlapping and the isotropic MR recovers. Similar to the case of the BIO film on DTO substrate, such results can be understood as the spins in DTO fail to follow the ice rule (2-in-2-out ground state) at elevated temperatures due to thermal fluctuations.

Having the nature of the anisotropic MR feature confirmed, the strain effects on DTO unfold through comparing the difference of the BIO/DTO/YSZ from the BIO/DTO in terms of its higher critical field and lower freezing temperature. Since the dipolar interaction is long range, we can anticipate its strain-induced modulation to be minimal. The most significant change due to the epitaxial strain is likely the Dy³⁺ nearest-neighbor antiferromagnetic exchange interaction, which is in competition with the dipolar interaction^{38, 39}. Studies on the dipolar spin ice model have shown that the antiferromagnetic interaction favors an all-in-all-out structure^{1, 6}. In the present case, the strain for a [111]-oriented layer is expected to differentiate the interactions within the Kagome lattice plane, J , and that links the Kagome and triangular lattice planes, J' , as shown in a schematic graph in figure 3(d). Such a disproportionation of the exchange interaction strength could destabilize the spin ice state under thermal fluctuations and at the same time suppress the field-induced 3-in-1-out state. For instance, a minimal model, where the magnitude of J' is enhanced relative to J due to the vertical compression in the BIO/DTO/YSZ heterostructure, would lead to effective weakening of the coupling between the Kagome and triangular lattice planes, leading to suppression of the three-dimensional spin ice state. It would also demand a larger external field to flip the moments in the Kagome planes because of a decreased internal field from the moments in the triangular planes. Since the triangular planes are already aligned by the field before the transition to the 3-in-1-out state, the result is a reinforcement of the Kagome spin ice state. These are consistent with the experimental observations that the critical field significantly increases from the BIO/DTO to the BIO/DTO/YSZ.

To summarize, we have successfully converted the emergent spin configuration of an insulating frustrated magnet into an electronic response by designing a pyrochlore heterostructure of the spin ice DTO and a bad metal BIO. An emergent MR anomaly is observed as a result of the breaking of the ice rule. A systematic comparison between the BIO film grown on a DTO single crystal and a bilayer heterostructure of BIO/DTO grown on YSZ substrate demonstrates the possibility of probing the exotic spin state in thin films of insulating quantum magnets. These results open a new avenue to designing, engineering, and probing novel non-conducting frustrated quantum materials with emergent magnetic properties.

Acknowledgement: This research is supported by the U. S. Department of Energy under grant No. DE-SC0020254. H. D. Z. and J. L. acknowledge support from the Organized Research Unit Program; the Electromagnetic Property Laboratory; the Scholarly Activity and Research Incentive Fund (SARIF) at the University of Tennessee. E. D. was supported by the US Department of Energy (DOE), Office of Science, Basic Energy Sciences (BES), Materials Sciences and Engineering Division. The synchrotron x-ray diffraction measurement used resources of the Advanced Photon Source, a U.S. Department of Energy (DOE) Office of Science User Facility operated for the DOE Office of Science by Argonne National Laboratory under Contract No. DE-AC02-06CH11357. A portion of this work was performed at the National High Magnetic Field Laboratory, which is supported by the National Science Foundation Cooperative Agreement No. DMR-1644779 and the state of Florida. The authors thank Martin Mourigal and his research group for providing help in resistivity measurements; Jenia Karapetrova for helping with the synchrotron x-ray diffraction; Cristian Batista and Jiun-Haw Chu for fruitful discussions.

Experimental Method:

Synthesis of the DTO single crystal: polycrystalline DTO was prepared by prepared by thoroughly mixing stoichiometric Dy_2O_3 and TiO_2 with the molar ratio of 1:2. Prior to weighing, Dy_2O_3 was preheated at 1000 °C for 10h in order to remove the moisture. After grinding the mixture, sintering the mixture at 1000 °C and 1400 °C for 20h each in air with intermediate grinding. The powders were then compressed to a feed rod which was used to grow the single crystal DTO by using a double elliptical mirror optical floating-zone furnace SC1-MDH from Canon Machinery. To avoid oxygen deficiency, we grew the single crystal in 5atm flowing O_2 atmosphere. In the first cycle we used a high growth rate of 50 mm/h for both feed and seed rods and in the second cycle we used a relatively slow growth rate of 4 mm/h.

Sample preparation: The DTO single crystal was first aligned by a HUBER Laue X-ray diffractometer and then cut into substrate pieces with DTO (111) lattice plane by using the Model 650 Low Speed Diamond Wheel Saw from South Bay Technology. The substrate surfaces were prepared by going through a five-step mechanical polishing process with monocrystalline

suspension. The surfaces were characterized by an MFP-3D Atomic Force Microscope from Asylum Research. Thin film samples were synthesized by Pulsed Laser Deposition²⁸.

X-ray characterization: In-house x-ray characterization was done by an Empyrean diffractometer at Copper radiation. Synchrotron x-ray diffraction was performed at beamline 33-BM at the Advanced Photon Source at the Argonne National Laboratory.

Resistivity and magnetoresistance measurements: Transport measurement was performed with a Physical Properties Measurement System (PPMS) from Quantum Design (QD). The current is applied along [1 1 -2] direction to make sure it is always perpendicular to the field direction. Magnetoresistance (MR) between 0.3 K and 0.95 K was measured with a Dilution Refrigerator (DR) of a PPMS Dynacool from QD. MR between 0.03 K and 0.3 K was measured at the National High Magnetic Field Laboratory, station SCM1. All MR data were measured by utilizing the lock-in technique. Samples used in the measurement are of 3 mm (W) × 6 mm (L) in dimension. The DTO single crystal and the YSZ substrate are of 0.5 mm in thickness.

AC susceptibility: AC susceptibility was measured at the National High Magnetic Field Laboratory, station SCM2, by utilizing the lockin technique.

Author contributions: H. D. Z and J. L. conceived the idea and directed the study. K. N. and C. K. X. performed the pulsed laser deposition. C. K. X. synthesized the single crystal substrates. K. N. and C. K. X. performed the surface preparation. L. H. and C. K. X. performed in-house x-ray scattering measurement. H. Z., L. H. and J. Y. performed synchrotron x-ray diffraction. H. Z., T. H. Z, Z. G. J., C. K. X., K. N., S. P. and E.S.C. performed the transport measurements. C. K. X. and Q. H. conducted the ac susceptibility measurement. H. Z., K. N., C. K. X., H. D. Z, and J. L. analyzed the data. H. Z., H. D. Z, and J. L. wrote the manuscript with contributions from all other authors.

Competing interests

The authors declare no competing interests.

Figure 1

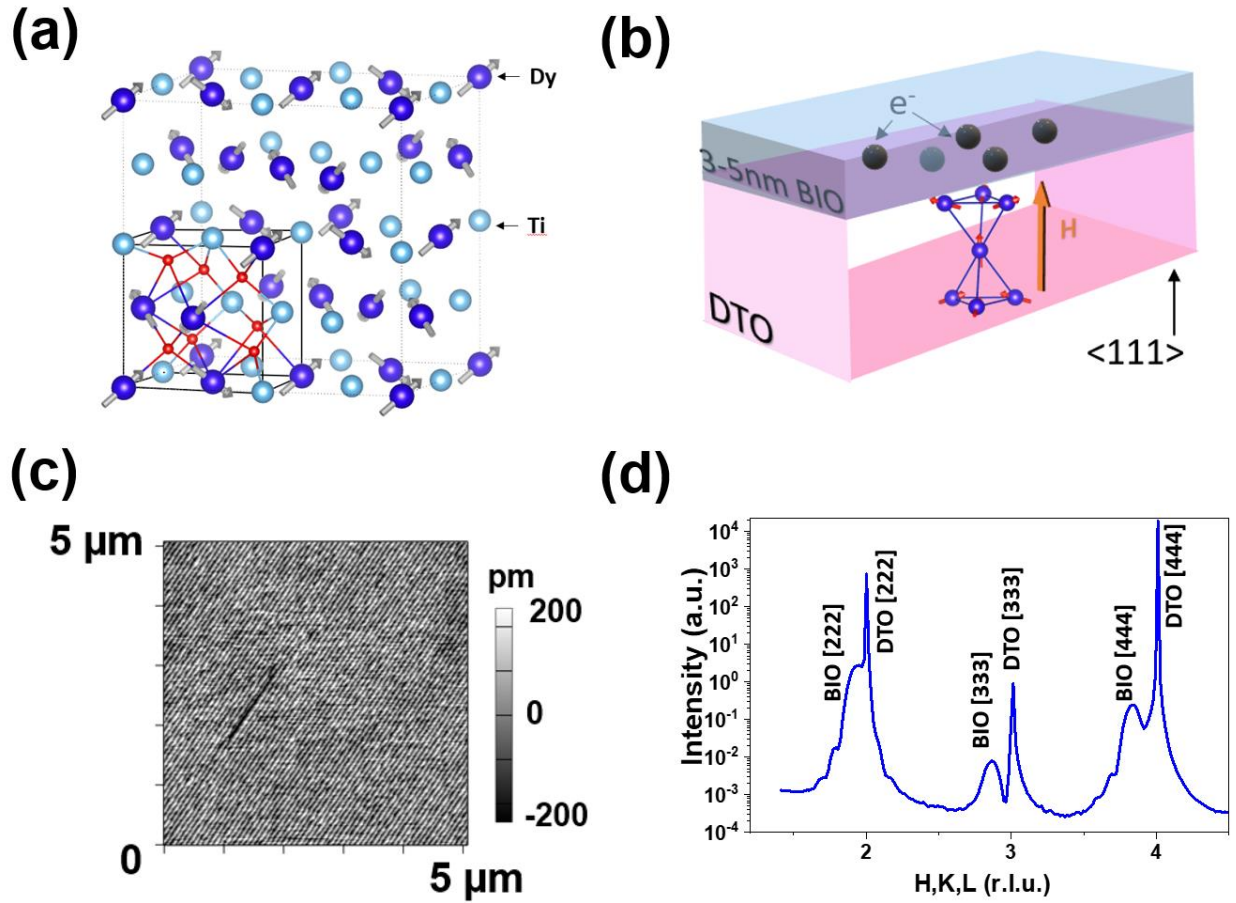


Figure 1 (a) crystal structure of $\text{Dy}_2\text{Ti}_2\text{O}_7$, the Dy and Ti atoms each form corner-sharing tetrahedra. Oxygen atoms outside the solid cube are not shown for clarity purpose. The spins on the Dy sites show the '2-in-2-out' configuration. (b) designed heterostructure with a 3-5nm BIO thin film deposited on the DTO single crystal. (c) The AFM image of the DTO substrate surface. (d) Synchrotron x-ray diffraction covering the DTO [222] to [444] region.

Figure 2

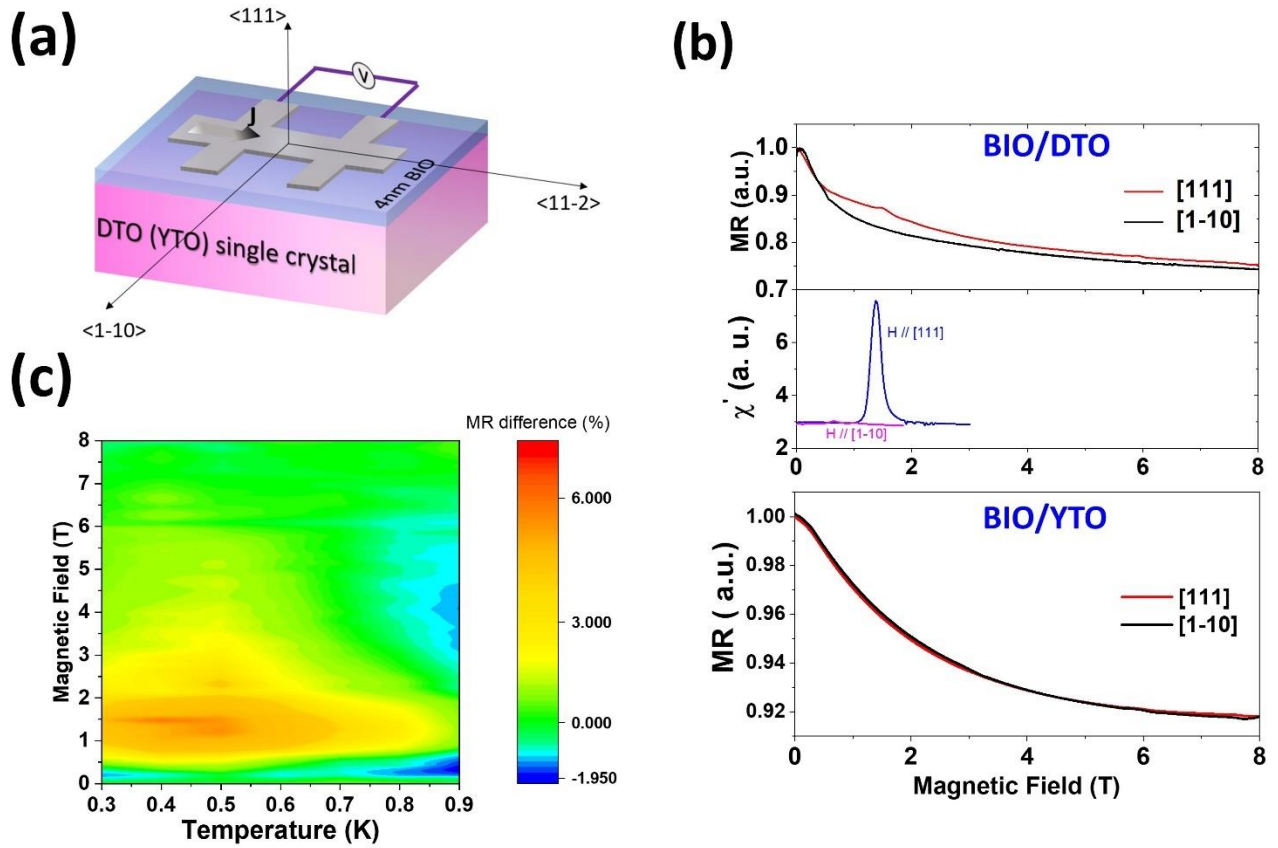


Figure 2 (a) schematic diagram of the measurement with BIO/DTO(YTO) heterostructure. (b) (top) measured MR for the BIO/DTO heterostructure at 0.3 K with $H // [111]$ (red) and $H // [1-10]$ (black), with AC susceptibility measured at the same temperature with $H // [111]$ (blue) and $H // [1-10]$ (pink). (bottom) MR for the BIO/YTO heterostructure shows no similar anomaly. (c) color plot of the MR difference with $H // [111]$ and $H // [1-10]$, measured between 0.3 K and 0.9 K.

Figure 3

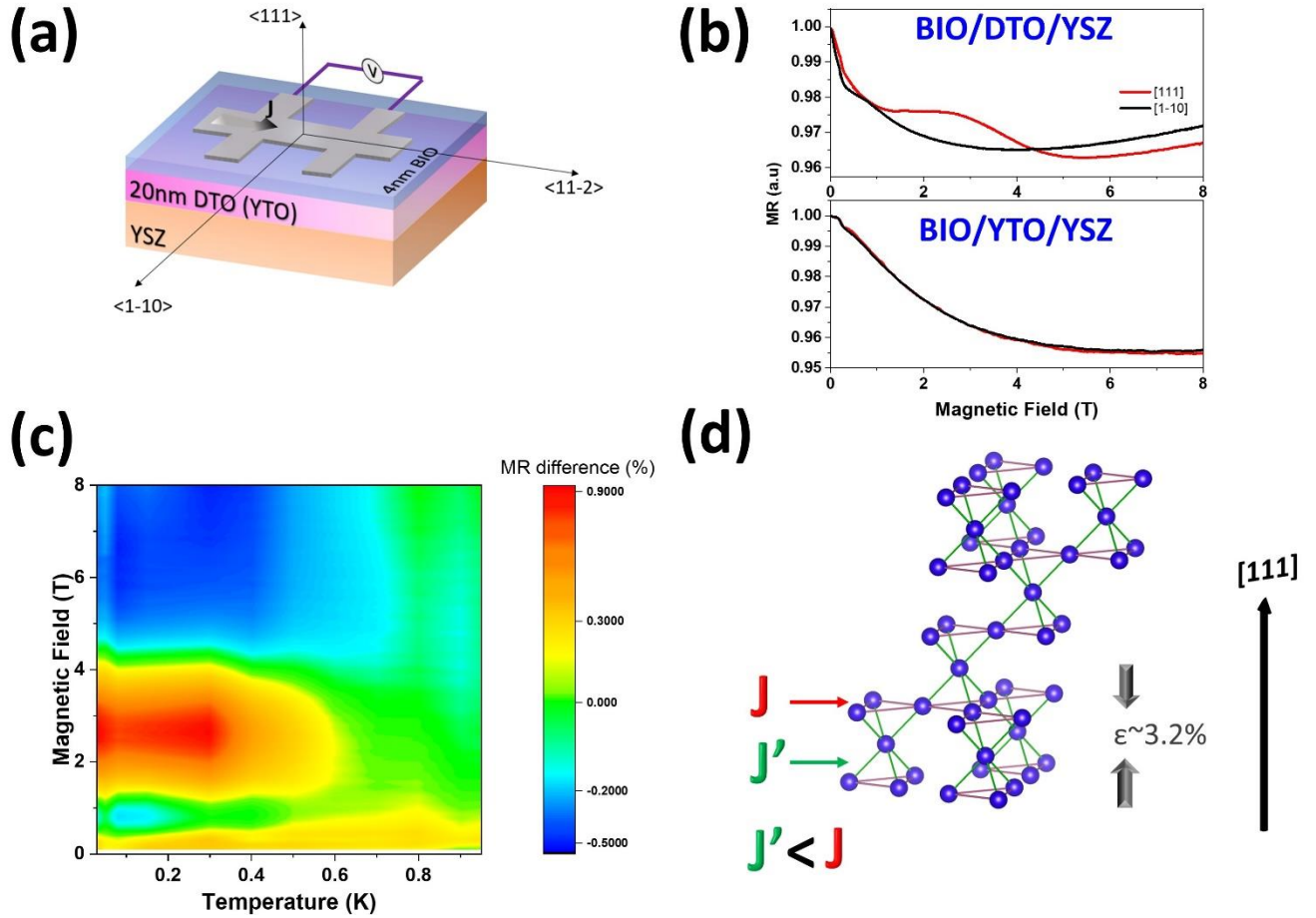


Figure 3 (a) schematic diagram of the measurement with BIO/DTO(YTO)/YSZ heterostructure (b) Magnetoresistance of the BIO/DTO/YSZ (top) and BIO/YTO/YSZ (bottom) heterostructure measured at 0.3 K. The external magnetic field is applied along the local $[1-10]$ (black) and $[111]$ (red) direction, respectively. (c) schematic diagram showing the epitaxial strain-induced change in the in- and out-plane exchange interaction J . (d) Color plot constructed by the percent difference of MR when field is along $[111]$, $[1-10]$ directions.

References

1. Lacroix C, Mendels P, Mila F. *Introduction to frustrated magnetism: materials, experiments, theory*, vol. 164. Springer Science & Business Media, 2011.
2. Castelnovo C, Moessner R, Sondhi SL. Spin Ice, Fractionalization, and Topological Order. *Annu Rev Condens Matter Phys* 2012, **3**(1): 35-55.
3. Gingras MJ, McClarty PA. Quantum spin ice: a search for gapless quantum spin liquids in pyrochlore magnets. *Rep Prog Phys* 2014, **77**(5): 056501.
4. Knolle J, Moessner R. A Field Guide to Spin Liquids. *Annu Rev Condens Matter Phys* 2019, **10**(1): 451-472.
5. Savary L, Balents L. Quantum spin liquids: a review. *Rep Prog Phys* 2017, **80**(1): 016502.
6. Gardner JS, Gingras MJP, Greedan JE. Magnetic pyrochlore oxides. *Rev Modern Phys* 2010, **82**(1): 53-107.
7. Melko RG, den Hertog BC, Gingras MJ. Long-range order at low temperatures in dipolar spin ice. *Phys Rev Lett* 2001, **87**(6): 067203.
8. Siddharthan R, Shastry BS, Ramirez AP, Hayashi A, Cava RJ, Rosenkranz S. Ising Pyrochlore Magnets: Low-Temperature Properties, "Ice Rules," and Beyond. *Phys Rev Lett* 1999: 1854.
9. Yavors'kii T, Fennell T, Gingras MJ, Bramwell ST. Dy₂Ti₂O₇ spin ice: a test case for emergent clusters in a frustrated magnet. *Phys Rev Lett* 2008, **101**(3): 037204.
10. Ruff JP, Melko RG, Gingras MJ. Finite-temperature transitions in dipolar spin ice in a large magnetic field. *Phys Rev Lett* 2005, **95**(9): 097202.
11. Bertin A, Chapuis Y, Dalmas de Reotier P, Yaouanc A. Crystal electric field in the R₂Ti₂O₇ pyrochlore compounds. *J Phys Condens Matter* 2012, **24**(25): 256003.
12. Ramirez AP, Hayashi A, Cava RJ, Siddharthan R, Shastry BS. Zero-point entropy in 'spin ice'. *Nature* 1999, **399**: 333.

13. Castelnovo C, Moessner R, Sondhi SL. Magnetic monopoles in spin ice. *Nature* 2008, **451**(7174): 42-45.
14. Tabata Y, Kadowaki H, Matsuhira K, Hiroi Z, Aso N, Ressouche E, *et al.* Kagome ice state in the dipolar spin ice $\text{Dy}_2\text{Ti}_2\text{O}_7$. *Phys Rev Lett* 2006, **97**(25): 257205.
15. Matsuhira K, Hiroi Z, T T, S T, Sakakibara T. A new macroscopically degenerate ground state in the spin ice compound $\text{Dy}_2\text{Ti}_2\text{O}_7$ under a magnetic field. *J Phys Condens Matter* 2002, **14**.
16. Sakakibara T, Tayama T, Hiroi Z, Matsuhira K, Takagi S. Observation of a liquid-gas-type transition in the pyrochlore spin ice compound $\text{Dy}_2\text{Ti}_2\text{O}_7$ in a magnetic field. *Phys Rev Lett* 2003, **90**(20): 207205.
17. Moessner R, Sondhi SL. Theory of the [111] magnetization plateau in spin ice. *Phys Rev B* 2003, **68**(6): 064411.
18. Yasui Y, Kondo Y, Kanada M, Ito M, Harashina H, Sato M, *et al.* Magnetic Structure of $\text{Nd}_2\text{Mo}_2\text{O}_7$. *J Phys Soc Jpn* 2001, **70**(1): 284-289.
19. Jiang Y, Huq A, Booth CH, Ehlers G, Greedan JE, Gardner JS. Order and disorder in the local and long-range structure of the spin-glass pyrochlore, $\text{Tb}_2\text{Mo}_2\text{O}_7$. *J Phys Condens Matter* 2011, **23**(16): 164214.
20. Lefrancois E, Simonet V, Ballou R, Lhotel E, Hadj-Azzem A, Kodjikian S, *et al.* Anisotropy-Tuned Magnetic Order in Pyrochlore Iridates. *Phys Rev Lett* 2015, **114**(24): 247202.
21. Wan X, Turner AM, Vishwanath A, Savrasov SY. Topological semimetal and Fermi-arc surface states in the electronic structure of pyrochlore iridates. *Phys Rev B* 2011, **83**(20).
22. Zhao S, Mackie JM, MacLaughlin DE, Bernal OO, Ishikawa JJ, Ohta Y, *et al.* Magnetic transition, long-range order, and moment fluctuations in the pyrochlore iridate $\text{Eu}_2\text{Ir}_2\text{O}_7$. *Phys Rev B* 2011, **83**(18): 180402.
23. Yang BJ, Nagaosa N. Emergent topological phenomena in thin films of pyrochlore iridates. *Phys Rev Lett* 2014, **112**(24): 246402.

24. Tian Z, Kohama Y, Tomita T, Ishizuka H, Hsieh TH, Ishikawa JJ, *et al.* Field-induced quantum metal–insulator transition in the pyrochlore iridate $\text{Nd}_2\text{Ir}_2\text{O}_7$. *Nat Phys* 2015, **12**(2): 134-138.
25. Sagayama H, Uematsu D, Arima T, Sugimoto K, Ishikawa JJ, O’Farrell E, *et al.* Determination of long-range all-in-all-out ordering of Ir^{4+} moments in a pyrochlore iridate $\text{Eu}_2\text{Ir}_2\text{O}_7$ by resonant x-ray diffraction. *Phys Rev B* 2013, **87**(10): 100403.
26. Matsuhira K, Tokunaga M, Wakeshima M, Hinatsu Y, Takagi S. Giant magnetoresistance effect in the metal–insulator transition of pyrochlore oxide $\text{Nd}_2\text{Ir}_2\text{O}_7$. *J Phys Soc Jpn* 2013, **82**(2): 023706.
27. Prabhakaran D, Boothroyd AT. Crystal growth of spin-ice pyrochlores by the floating-zone method. *J Cryst Growth* 2011, **318**(1): 1053-1056.
28. Chrisey DB, Hubler GK. Pulsed laser deposition of thin films. 1994.
29. Cao G, Schlottmann P. The challenge of spin-orbit-tuned ground states in iridates: a key issues review. *Rep Prog Phys* 2018, **81**(4): 042502.
30. Shinaoka H, Hoshino S, Troyer M, Werner P. Phase Diagram of Pyrochlore Iridates: All-in-All-out Magnetic Ordering and Non-Fermi-Liquid Properties. *Phys Rev Lett* 2015, **115**(15): 156401.
31. Zhang H, Haule K, Vanderbilt D. Metal-Insulator Transition and Topological Properties of Pyrochlore Iridates. *Phys Rev Lett* 2017, **118**(2): 026404.
32. Qi TF, Korneta OB, Wan X, DeLong LE, Schlottmann P, Cao G. Strong magnetic instability in correlated metallic $\text{Bi}_2\text{Ir}_2\text{O}_7$. *J Phys Condens Matter* 2012, **24**(34): 345601.
33. Chu J-H, Liu J, Zhang H, Noordhoek K, Riggs SC, Shapiro M, *et al.* Possible scale invariant linear magnetoresistance in pyrochlore iridates $\text{Bi}_2\text{Ir}_2\text{O}_7$. *New J Phys* 2019, **21**(11): 113041.
34. Yang W, Xie Y, Zhu W, Park K, Chen A, Losovyj Y, *et al.* Epitaxial thin films of pyrochlore iridate $\text{Bi}_{2+x}\text{Ir}_{2-y}\text{O}_{7-\delta}$: structure, defects and transport properties. *Sci rep* 2017, **7**(1): 1-11.
35. Leusink DP, Coneri F, Hoek M, Turner S, Idrissi H, Van Tendeloo G, *et al.* Thin films of the spin ice compound $\text{Ho}_2\text{Ti}_2\text{O}_7$. *APL Mater* 2014, **2**(3).

36. Barry K, Zhang B, Anand N, Xin Y, Vailionis A, Neu J, *et al.* Modification of spin-ice physics in $\text{Ho}_2\text{Ti}_2\text{O}_7$ thin films. *Phys Rev Mater* 2019, **3**(8).
37. Lantagne-Hurtubise É, Rau JG, Gingras MJP. Spin-Ice Thin Films: Large-N Theory and Monte Carlo Simulations. *Phys Rev X* 2018, **8**(2): 021053.
38. Bovo L, Moya X, Prabhakaran D, Soh YA, Boothroyd AT, Mathur ND, *et al.* Restoration of the third law in spin ice thin films. *Nat Commun* 2014, **5**: 3439.
39. Savary L, Wang X, Kee H-Y, Kim YB, Yu Y, Chen G. Quantum spin ice on the breathing pyrochlore lattice. *Phys Rev B* 2016, **94**(7).